Journal of Materials and Environmental Sciences
ISSN : 2028-2508

JMES, 2017 Volume 8, Issue 8, Page 3013-3027

http://www.jmaterenvironsci.com

Analysis of combined natural convection and thermal radiation heat transfer in a triangular shaped roof for hot climates

A. Amrani[1,2*], N. Dihmani[1], S. Amraqui[1], A. Mezrhab[1]

[1]*Université Mohammed Premier, Faculté des Sciences, Laboratoire de Mécanique & Energétique, 60000 Oujda, Maroc.*
[2]*Département de Physique, Faculté des Sciences et Techniques, BP 509 Boutalamine,52000 Errachidia, Maroc.*

Received 05 Jun 2016,
Revised 30 Aug 2016,
Accepted 26 Oct 2016

Keywords

- ✓ Finite volume method
- ✓ Gabel roof,
- ✓ Natural convection,
- ✓ Surface radiation,
- ✓ Triangular shaped roof

am.abdelillah@gmail.com
Phone: +212672962357

Abstract

The roofs play an important role in the energy performance of building. In the present study, natural convection with surface radiation heat transfer is investigated numerically in a triangular shaped roof with eave (Gabel roof) for hot climates. A specifically developed numerical model, based on the finite-volume method, is used for the solutions of the governing differential-equations. The SIMPLER algorithm was adopted for the treatment of velocity-pressure coupling. Concerning the radiation exchange, we consider that the fluid (air) is transparent, so only the solid surfaces contribute to the radiation exchange and assumed to be diffuse-gray. The key parameters for this analysis are considered as Rayleigh number (*Ra*), aspect ratio (*A*) and eave lengths (e^*). Results are reported in terms of isotherms, streamlines and local and average Nusselt numbers.

1. Introduction

Natural convection heat transfer and fluid flow in triangular enclosures has been a subject of interest in many diverse fields of applications. Some of these applications are as follows: building and thermal insulation systems, Solar engineering applications, electronic equipment cooling, Geophysical fluid mechanics, etc. [1-4].

Over the year, many experimental and numerical studies have been reported in textbooks, articles and technical documents. One of the first studies about laminar natural convection in triangular enclosures was a solely experimental study made in 1979 by Flack et al. [5], an enclosure with the cross-section of an isosceles triangle was considered the base of which was insulated and the inclined walls were isothermal. Both local and overall heat transfer data were obtained by the use of a Wollaston prism schlieren interferometer. It is shown that there are high temperature gradients near the surfaces, with liquid stratification occurring in the central part of the enclosure. A numerical study in right triangular enclosures was performed by Akinsete and Coleman [6]. The base, the inclined wall and the vertical wall of the enclosure was assumed to be cooled, heated and adiabatic respectively. They concluded that heat transfer across the base wall increases towards the hypotenuse and base intersection. It was found that a considerable proportion of the heat transfer across the base wall of the region takes place near the intersection of the base and the hypotenuse.

Moreover, Karyakin and Sokovishin [7] presented natural convection patterns in isosceles triangular enclosure. Two cases of thermal boundary conditions are considered: (a) the horizontal base is adiabatic, while the inclined walls are isothermal (cold and hot); (b) all the solid surfaces are isothermal (hot inclined surfaces and cold bottom). They observed that the maximum values of stream functions and Nusselt numbers perform damping oscillations around the steady state values. At high *Gr*, gradient regions of the type of dynamic and thermal boundary layers are formed on all the solid surfaces and the temperature distribution in the central part of the enclosure approaches the conditions of fluid stratification. Kaushik et al. [8] studied the performance of a triangular built-in-storage solar water heater under winter conditions. The forward finite difference technique is employed and initial conditions are derived from the assumption that the water temperature and the temperature at each node are in equilibrium with the ambient temperature. They proved that triangular cross-section of the system results in higher solar gain and enhance the natural convection leading to higher water temperature. Salmun [9] studied the problem of natural convection inside a two dimensional triangular geometry filled with air or water, with various aspect ratios and Rayleigh numbers. Following the earlier simulations, only half of the domain was examined. The center plane was insulated and this was thought to adequately model the entire

domain. The transient numerical experiments show that in the present parametric domain the single-cell circulation is not stable with respect to the Bernard instability one expects in fluid layers heated from below.

Recently, Holtzman et al. [10] revealed that the natural convection flow in an isosceles triangular domain undergoes a transition from symmetric to asymmetric structures. For low Grashof numbers, their numerical solutions show symmetric structures about the geometric plane of symmetry with single-cell structures on both sides of the mid-plane. As the Grashof number increases above a critical value, the symmetric solutions become unstable, and asymmetric solutions are obtained. Lei and Patterson [11] carried out a model experiment to visualize the convection process in a shallow triangular cavity. This study consists of two parts: a scaling analysis and a numerical simulation. The scaling analysis for small bottom slopes reveals that a number of flow regimes are possible depending on the Rayleigh number and the relative value of certain non-dimensional parameters describing the flow. In a typical situation, the flow can be classified broadly into a conductive, a transitional or a convective regime determined merely by the Rayleigh number.

In another study, Ridouane and Campo [12] compared the isosceles, right-angled triangles and rectangular enclosure to maximize the convection heat transport in cavities and minimize their sizes. They observed that the airflow remains symmetric for the isosceles triangular cavity even at high Grashof numbers. Natural convection heat transfer has been analyzed numerically in a right-angled triangular enclosure with flush mounted heat on the vertical wall, by Varol et al [13]. Finite difference method is used in solution of governing equations in stream function-vorticity form. They have examined the effect of Aspect ratio, Rayleigh number and location and length of heater. They have found that among these parameters, position of heater is the most important parameter and can be considered a control parameter.

In 2007, Saha et al. [14] studied natural convection within a tilted isosceles triangular enclosure with discrete bottom heating. The two upper walls are maintained at constant cold temperature, whereas a constant heat flux is symmetrically embedded at the bottom wall, and the non-heated parts of the bottom wall are considered adiabatic. They observed that the average Nusselt number decreases with increase in length of the heat strip and increases with inclination angle φ. The effect of Prandtl number on natural convection heat transfer and fluid flow in triangular enclosures with localized heating has been analyzed by Koca et al. [15]. Temperature of inclined wall is lower than the temperature of the heater while remaining walls are adiabatic. Aspect ratio of triangle was chosen as unity. The results show that the heat transfer increases when heater length, Prandtl number, Rayleigh number increase and when heater was located near the right corner. Varol et al. [16] studied numerically the natural convection heat transfer from a protruding heater located in triangular enclosure. Temperature of inclined wall of triangle was lower than the temperature of the heater, while the remaining wall was insulated. Various Rayleigh number, aspect ratio of triangle enclosure, dimensionless size (height and width) of heater and dimensionless location were examined. It is shown that all parameters related with geometrical dimensions of the heater are effective on temperature distribution, flow field and heat transfer. Finally, Saha [17] investigated the fluid flow and heat transfer inside a triangular enclosure due to instantaneous heating on the inclined walls. The development of the unsteady natural convection boundary layer under the inclined walls may be classified into three distinct stages including a start-up stage, a transitional stage and a steady state stage, which can be clearly identified in the analytical and numerical results.

One important application of this type of geometry which has a great interest of many researchers recently is the natural convection through triangular shaped roofs (Gabel roofs) of buildings. Relatively, the numbers of studies on natural convection in triangular shaped roofs are very limited. In the studies of Asan and Namli [18], the laminar natural convection heat transfer in triangular shaped roofs with different inclination angle and Rayleigh number in summer day conditions is investigated numerically using finite volume method. They indicated that the height-to-base ratio has a profound influence on the temperature and flow field. On the other hand, the effect of Rayleigh number is not significant for $H/B < 1$ and $Ra < 10^5$. Ridouane et al. [19] compared the solution of two different boundary conditions for isosceles triangular cavity representative of conventional attic spaces in houses and buildings with pitched roofs and horizontal suspended ceilings. Tzeng et al. [20] proposed the numerical simulation aided parametric analysis method to solve natural convection equations in streamline-vorticity form. Then, they applied this method to laminar natural convection in triangle shaped roof. Finally, they developed a correlations for parameters which effective on flow and heat transfer.

Further, Koca [21] and Varol et al. [22] investigated the natural convection in different roof shapes including Gambrel and Saltbox roofs. They observed that natural convection flow fields strongly depend on the geometrical shape and thermal boundary conditions of the roof. Natural convection of different shapes of roof has also been investigated by Varol et al. [23]. The geometry adapted to both winter day conditions and summer day conditions. Most of the earlier works have been dealt for $Pr < 1$ and the dependency of Prandlt number was not clearly reported. The focus of this study is to establish scaling relations of the governing parameters for an

isosceles triangular enclosure with symmetric temperature boundary conditions on the slopping walls and adiabatic bottom wall for $Pr > 1$. The new scaling handles the dependency of Pr on the fluid flow and heat transfer very well.

All of the above studies pertain to natural convection heat transfer in triangular enclosures or triangular shaped roofs. Comparatively, few studies have been undertaken on the radiation exchange in triangular enclosures. Among the few studies carrying out on this kind of configurations and taking into account the radiation exchange, we can cite the one of Yadan Maa et al. [24]. The numerical simulation reveals three possible distinct flow regimes in the enclosure. It also reveals the variations of the dominant heat transfer mode and the flow status with the horizontal position along the wedge. For small Rayleigh numbers, heat transfer over the entire domain is dominated by conduction. For medium Rayleigh numbers, there are two distinct regions. Heat transfer in the near shore region is dominated by conduction. As the distance from the shore increases, stable convection becomes the dominant mode. The region dominated by stable convection expands with increasing Rayleigh number. For high Rayleigh numbers, the whole region can be divided into three distinct regions where the dominant mode of heat transfer changes from conduction to stable convection and then to unstable convection as the distance from the shore increases. The region of flow instability also expands with increasing Rayleigh number. In addition to Yadan Maa's study, Sieres et al. [25] studied laminar natural convection with and without surface-to-surface radiation in an upright right-angled triangular cavity filled with air. The vertical walls are uniformly heated and the inclined walls are uniformly cooled while the upper connecting walls are adiabatic. Overall, they found that the competition between surface radiation and natural convection in right-angled triangular cavities filled with air plays a preponderant role. Finally, the analysis culminates with the construction of a comprehensive correlation equation for the total Nusselt number in terms of the controlling parameters which should be useful for engineering analysis and design. This correlation equation will undoubtedly provide a fast evaluation avenue to judge the cavity thermal performance.

On the basis of the literature review, it appears that no work was reported on coupled natural convection and thermal radiation heat transfer in triangular shaped roofs (Gabel roofs). Thereafter, due to its practical interest in buildings, the subject needs further effort to improve the knowledge in this field. Hence, the objective of this work is to present a numerical investigation of steady combined laminar natural convection and surface radiation in a two-dimensional triangular shaped roof for various Rayleigh number (Ra), aspect ratio (A) and eave lengths (e^*).

2. Mathematical modelling and analysis

2.1. *Description of the physical model*

In the present study, the geometric configuration of a triangular shaped roof with eave (Gabel roof) is presented in figure 1. It is considered that the vertical wall is adiabatic with height h. The inclined surface and eave are heated at a constant temperature T_h. The bottom surface of the roof (room ceiling) with length b has constant cold temperature T_c. The length of eave is depicted by e.

The flow is assumed to be incompressible, laminar and two dimensional in a triangular shaped roofs. Thermophysical properties of the fluid (air) in the flow field are assumed to be constant at the average temperature T_0 except the density variations causing a body force term in the momentum equation. The walls of the roof are grey diffuse emitters and reflectors of radiation.

2.2. *Mathematical modelling*

Using the dimensionless variables defined in the nomenclature, governing dimensionless equations are obtained as:

* Continuity:
$$\frac{\partial U}{\partial X}+\frac{\partial V}{\partial Y}=0 \tag{1}$$

* X momentum:
$$U\frac{\partial U}{\partial X}+V\frac{\partial U}{\partial Y}=-\frac{\partial P}{\partial X}+Pr\left(\frac{\partial^2 U}{\partial X^2}+\frac{\partial^2 U}{\partial Y^2}\right) \tag{2}$$

* Y momentum:
$$U\frac{\partial V}{\partial X}+V\frac{\partial V}{\partial Y}=-\frac{\partial P}{\partial Y}+Pr\left(\frac{\partial^2 V}{\partial X^2}+\frac{\partial^2 V}{\partial Y^2}\right)+Ra\ Pr\,\theta \tag{3}$$

* Energy:
$$U\frac{\partial \theta}{\partial X}+V\frac{\partial \theta}{\partial Y}=\left(\frac{\partial^2 \theta}{\partial X^2}+\frac{\partial^2 \theta}{\partial Y^2}\right) \tag{4}$$

Hot and cold walls are maintained at dimensionless temperature of 0.5 and -0.5 respectively.

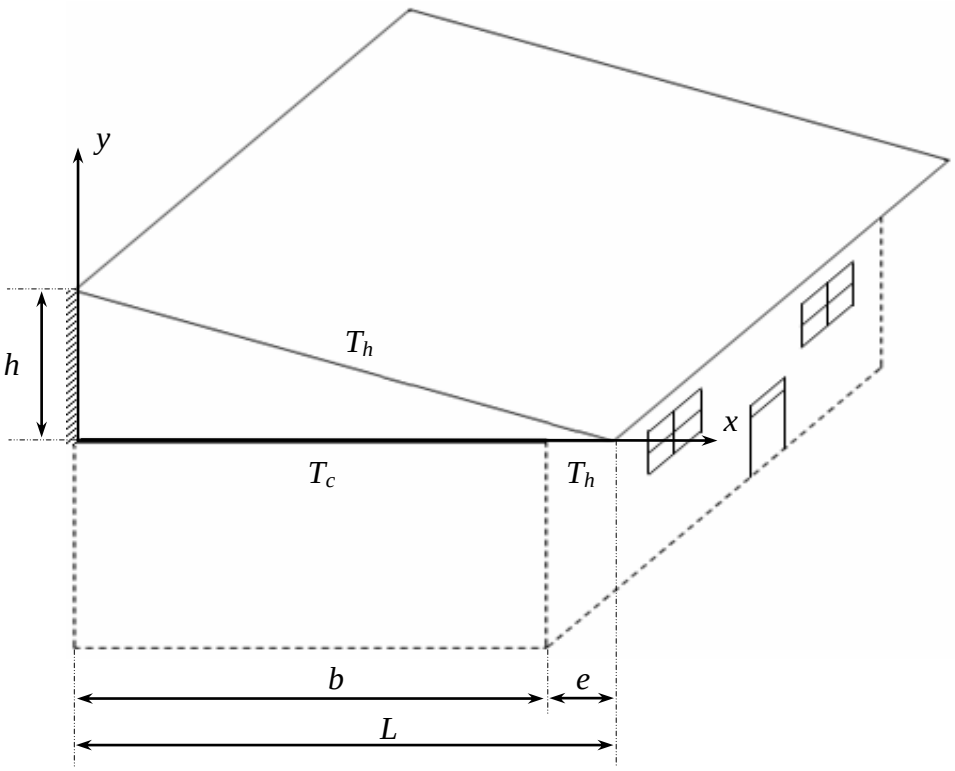

Figure 1. Geometry of the triangular shaped roofs (Gabel roofs).

The dimensionless boundary conditions corresponding to the considered problem are as follows:

- For the vertical wall, $X = 0$ and $0 \leq Y \leq 1$:

$$U = V = 0,\ \frac{\partial \theta}{\partial X} - Nr\phi_r = 0 \tag{5}$$

- For the inclined surface :

$$U = V = 0,\ \theta = 0.5 \tag{6}$$

- For the eave, 1- $b^* \leq X \leq 1$ and $Y = 0$:

$$U = V = 0,\ \theta = 0.5 \tag{7}$$

- For the bottom wall, $0 \leq X \leq 1$- b^* and $Y = 0$:

$$U = V = 0,\ \theta = -0.5 \tag{8}$$

The solid radiative surfaces forming the roofs are divided into a number of surfaces S_i, (i = 1, N). N is the number of total radiative surfaces forming the channel and the plate; which are equal to the total control volume interfaces solid-air. In fact, the control volume faces were also arranged so that a control volume face coincided with an interface solid-fluid. Therefore, the dimensionless net radiative flux density along a diffuse grey and opaque surface S_i is expressed as:

$$\phi_{r,i} = R_i - \sum_{j=1}^{N} R_j\ F_{ij} \tag{9}$$

Where the dimensionless radiosity is defined as:

$$\sum_{j=1}^{N} \left(\delta_{ij} - (1 - \varepsilon_i)\, F_{ij} \right) R_j = \varepsilon_i\, \Theta_i^4 \tag{10}$$

The heat transfer rate by natural convection and surface radiation in triangular shaped roofs is obtained from the average Nusselt number calculation. The local Nusselt number over the bottom surfaces are expressed as:

$$Nu(X,\ Y = 0) = Nucv(X,\ Y = 0) + Nur(X,\ Y = 0) \tag{11}$$

Where *Nucv* and *Nur* are the convective and radiative contributions in *Nuw*. The average Nusselt number is the average of local Nusselt number along the bottom surface and is defined by the following equation:

$$Num = \frac{1}{A} \int_0^A \left(-\left. \frac{\partial \theta}{\partial Y} \right|_{X,\ Y=0} + Nr\, \phi_r \left(X,\ Y = 0 \right) \right) dX \tag{12}$$

2.3. *Numerical technique (grid)*

The governing equations reported above are discretized on a staggered, non-uniform Cartesian grid using a finite-volume procedure with a central differencing scheme (CDS) for the convective terms. The SIMPLER algorithm is employed for the velocity–pressure coupling [26]. The iterative process is repeated until steady state: max $\left|\phi^{(n+1)}-\phi^{(n)}\right|<\varepsilon_{\chi}$ where χ is a dependent variable and n is the iteration number. In this study, the velocity components and temperature were driven to $\varepsilon_u=\varepsilon_v=\varepsilon_\theta<10^{-6}$ and for pressure $\varepsilon_p<10^{-8}$. The resulting systems of discretized equations were solved by a conjugate gradient method.

For the combined convection and radiation problem, the radiative surfaces temperatures of the adiabatic walls were calculated from the non-linear equation (Eqs. (5)) by using an inner iterative procedure at every time step for energy equation. At each inner iteration, the linear system of the radiosities equations (Eq. 10) is solved by a direct method (Gauss elimination). Indeed, the grid was constructed such that the boundaries of physical domain coincided with the velocity grid lines. The points for pressure and temperature were placed at the center of the scalar volumes. At the fluid-solid interfaces, the control volume faces were also arranged so that a control volume face coincided with an interface solid-fluid. Therefore, the zoning was not uniform and the area of each zone varied according to the stretching function and number of grid points used. This grid distribution was chosen to ensure the interface energy balance. To avoid a checkerboard pressure and velocity field a staggered grid for velocity is used.

Since the radiative flux leaving the solid surfaces vary from point to the other (even on the isothermal side-walls because the incident radiation cannot be assumed as uniform), each of the surfaces was divided into finite number of zones on which the four basic assumptions of the simplified zone analysis was assumed valid. The number of zones retained was determined by the mesh used to solve the differential equations. Therefore, the zoning was no uniform and the area of each zone varied according to the stretching function and number of grid points used. For N radiative surfaces, this results in $N(N\text{-}1)/2$ view factors to be calculated and in a linear system of N equations for the radiosities. The view factors were determined by using a boundary element approximation to fit the surfaces and a Monte Carlo method for the numerical integrations [27].

Various computations were performed for A = 1, e^* = 1/3 and Ra = 10^5 for different uniform grids ($Nx\times Ny$) in order to examine the grid independence. Table 1 present the results for average Nusselt number Nuw and maximum stream function Ψ_{max}. Indeed, the maximum difference between the values of Nuw and Ψ_{max} obtained for the 120×120 grid and the finest 160×160 grid was less than 0.78%, and 0.76 % respectively. Consequently, to optimize appropriate grid refinement with computational efficiency, the grid 120×120 was chosen for all the further computations.

Table 1. Grid independence study in the pure natural convection case (ε = 0) for Pr = 0.71, A = 1, e^* = 1/3 and Ra = 10^5.

$(Nx\times Ny)$	Nuw	Ψ_{max}
40×40	2.325	2.0683
50×50	2.442	2.2473
60×60	2.542	2.3939
70×70	2.598	2.5503
80×80	2.648	2.6839
90×90	2.699	2.8059
100×100	2.728	2.9148
110×110	2.757	2.9932
120×120	2.790	3.0349
130×130	2.798	3.0380
140×140	2. 803	3.0434
150×150	2.808	3.0492
160×160	2.812	3.0582

3. Results and discussion

3.1 *Code validation*

Before presenting and discussing the obtained results, we present the validation of our code based on the finite volume method. It was extensively exercised on benchmark problems to check its validity (see [28-30]).

In one hand, the validation is achieved by comparing our results, in case of pure natural convection, with those obtained by with Asan and Namli [28] and Koca et al. [29]. The variation of the average Nusselt number versus Rayleigh number is shown in table 2. As can be seen, an excellent agreement is observed between our results and those of references [28-29].

Table 2. Comparison of mean Nusselt numbers for $e = 0$, $\varepsilon = 0$ and $A = 1$ with Asan and Namli [28] and Koca et al. [29].

Ra	10^3	10^4	10^5	10^6
Nuw (Asan and Namli [28])	4.87	5.12	7.15	12.27
Nuw (Koca et al. [29])	4.65	4.92	7.04	12.10
Nuw (Our results)	4.76	5.01	7.11	12.16

In figure 2, the local Nusselt number *Nu* for different values of aspect ratios *A* along the bottom wall is presented. It should be noted that the present results are compared with the results of [29] obtained for $e^* = 1/5$ and $Ra = 10^6$. As can be seen, the figure compare favorably with this reported by Koca et al. [29].

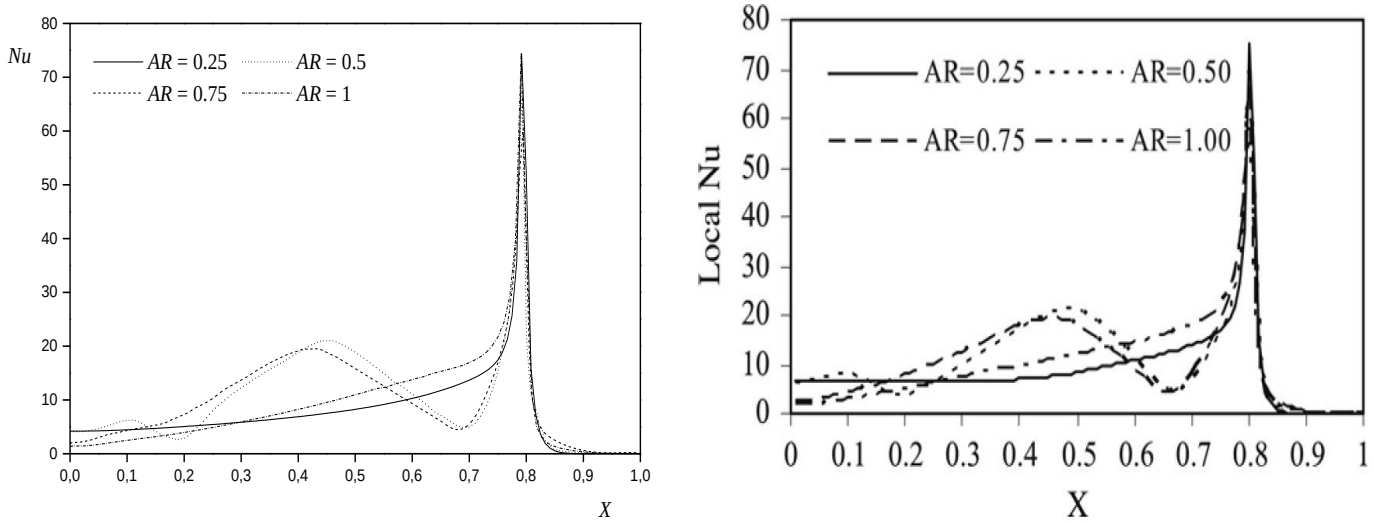

Our results Results of Koca et al. [29]

Figure 2. Variation of local Nusselt number for different aspect ratios along the bottom wall, $e^* = 1/5$, $Ra = 10^6$ and $\varepsilon = 0$.

In the other hand, the code was validated in case of radiation exchange for the transparent fluid in cavity as shown by Bouali et al. in [30]. Also, we have compared the results obtained by our code to those of Mezrhab et al. [31] for a heated horticultural greenhouse. It was concluded that the largest discrepancies between our results and published results can be estimated to be less than 1%. For this reason and for the sake of brevity, it is not repeated here. Consequently, the code gives excellent results that are in a good agreement with those obtained with other numerical results.

3.2 *Results and discussion*

In the following, numerical results obtained with air as a fluid ($Pr = 0.71$) are presented and discussed. The average temperature T_0 is chosen equal to 300 *K* and in order to keep available the Boussinesq approximation ($\Delta T < 0.1T_h$), the terminal temperature difference ΔT is kept equal to 30 *K*. For the remaining parameters (Rayleigh number *Ra*, aspect ratio *A* and eave lengths e^*) a detailed parametric study has been

carried out to investigate those effects on the heat transfer and the air flow in the triangular roof. We suppose that emissivities of all radiative surfaces are equal to 0 in pure natural convection and 1 in presence of the radiation exchange.

3.2.1. *Effect of Rayleigh number*

Figure 4 presents the isotherms and streamlines for different Rayleigh numbers and for aspect ratio and eave length fixed respectively to 0.5 and 1/3 in the absence ($\varepsilon = 0$) and in the presence ($\varepsilon = 1$) of radiation exchange. In case of pure natural convection (figure 4.a), we can note that, for small *Ra*, since the intensity of the buoyancy-driven convection is very weak the thermal field is thus unaffected. Increasing *Ra* will increase the dominancy of the convection on the transport. The streamlines form a nearly centrally located single cell and corresponding isotherms exhibit the characteristics of pure conduction. As Rayleigh number increases ($Ra \geq 10^5$), the general structure of the streamlines does not deteriorate but the center of the cell forms an elliptical shape. In the natural convection mode combined to the surface radiation(figure 4.b), we can note that isotherms structures near the solid surfaces are affected by thermal radiation and for this reason the isotherms are inclined near adiabatic solid surfaces whereas they are perpendicular in the pure natural convection mode. This inclination is more important as Rayleigh number increases. This is explained by the fact that the radiation number *Nr* is proportional to Rayleigh number. Also we can observe that, while increasing Rayleigh number, the temperature distribution and fluid flow is similar to the one observed in the pure natural convection. The streamlines structures indicate that the thermal radiation enhances the velocity flow in the roof.

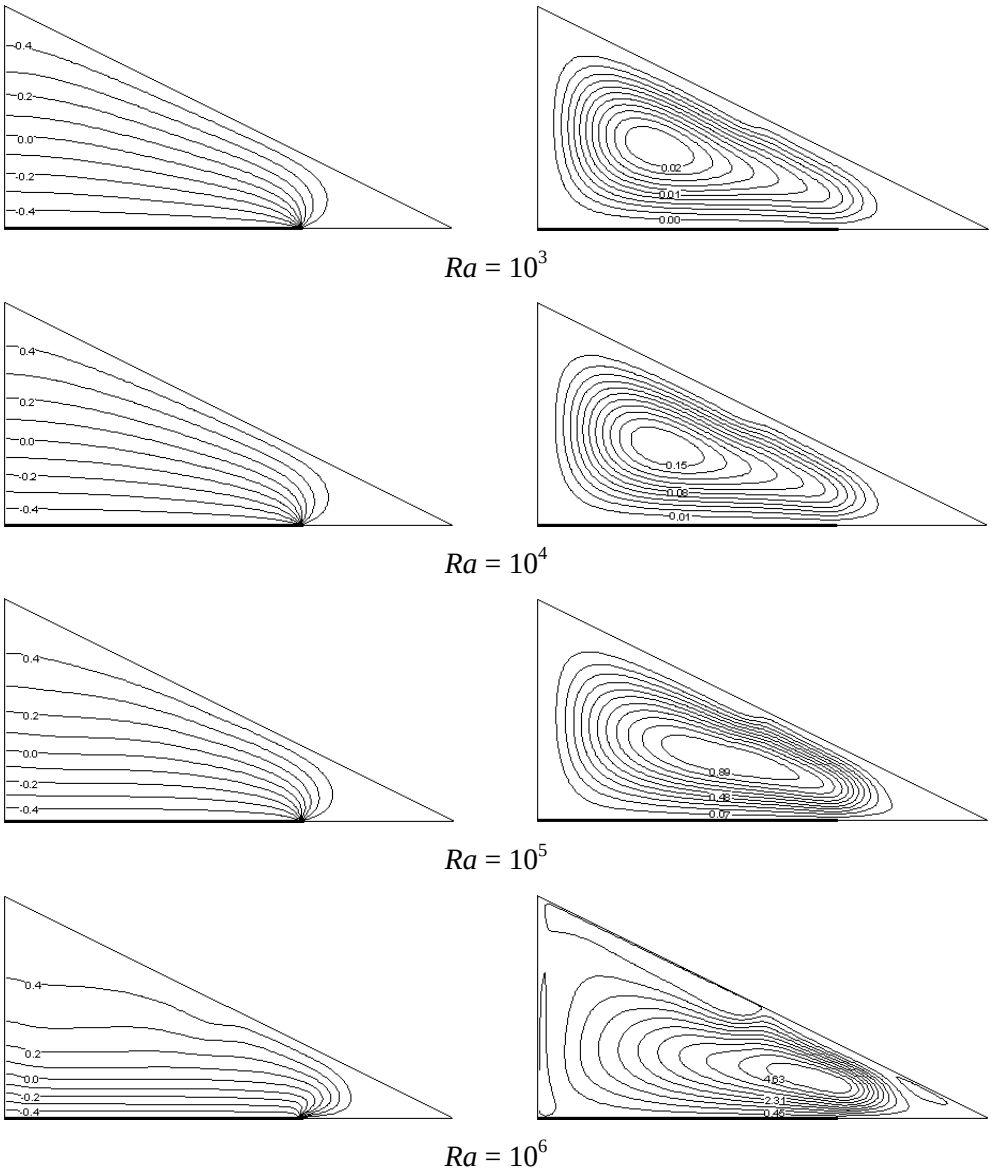

Figure 4.a. Isotherms and streamlines for different Rayleigh number and for $A = 0.5$, $e^* = 1/3$ and $\varepsilon = 0$.

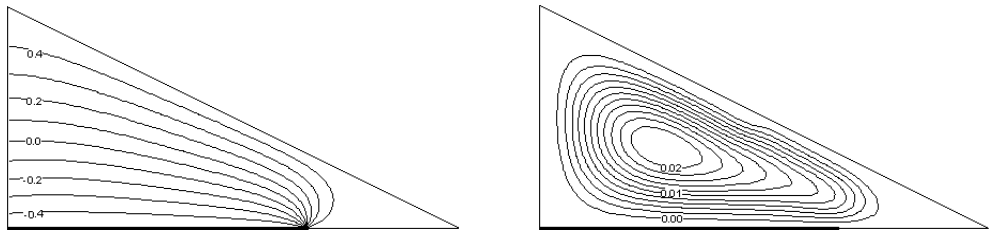

$Ra = 10^3$

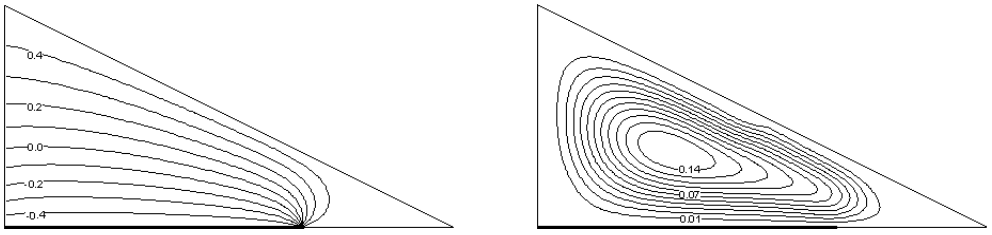

$Ra = 10^4$

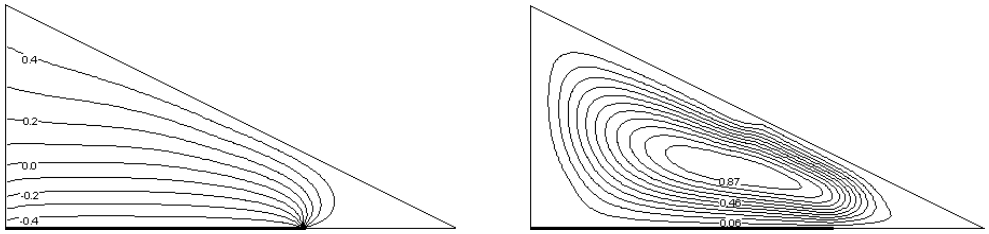

$Ra = 10^5$

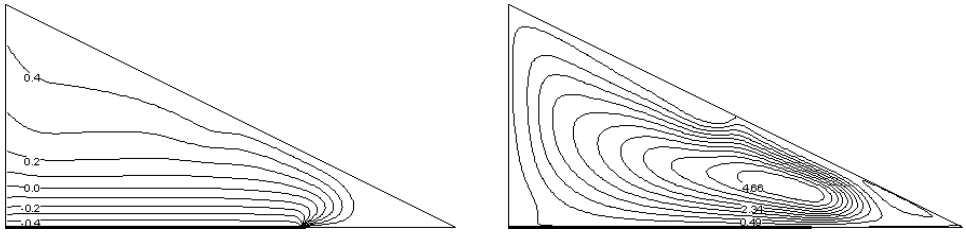

$Ra = 10^6$

Figure 4.b. Isotherms and streamlines for different Rayleigh number and for $A = 0.5$, $e^* = 1/3$ and $\varepsilon = 1$.

3.2.2. *Effect of aspect ratio*

The effect caused by the variation of the aspect ratio, on the isotherms and streamlines in absence and in presence of the surface radiation, are presented in figure 5 for $e^* = 1/3$ and $Ra = 10^5$.

In the two case ($\varepsilon = 0$ and $\varepsilon = 1$) we can note that there are significant changes of flow and heat transfer during the variation of aspect ratio. In one side, it is noted that when the aspect ratio decreases, the air circulation in the entire computational domain decreases. In all cases, there are one rotating cell except for $A = 0.25$ where we can observe formation of a secondary cell. However, this smaller cell is located at the bottom corner of the triangle. In the other side, isotherms have equal intervals between -0.5 and +0.5 which correspond to temperature of cold and hot wall respectively, especially for low value of aspect ratio. In more, the isotherms are parallel to the bottom wall and nearly follow the shape of the inclined wall.

Nevertheless, we can see the effect of radiation exchange on the isotherms where they become inclined near the adiabatic walls. And the temperature is homogenized in the triangular roof. The figure below will show this effect more clearly.

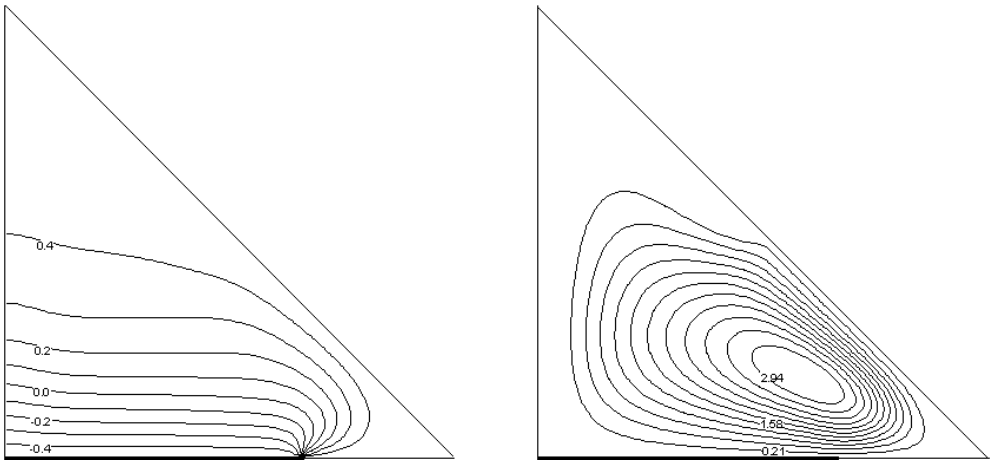

$A = 1$

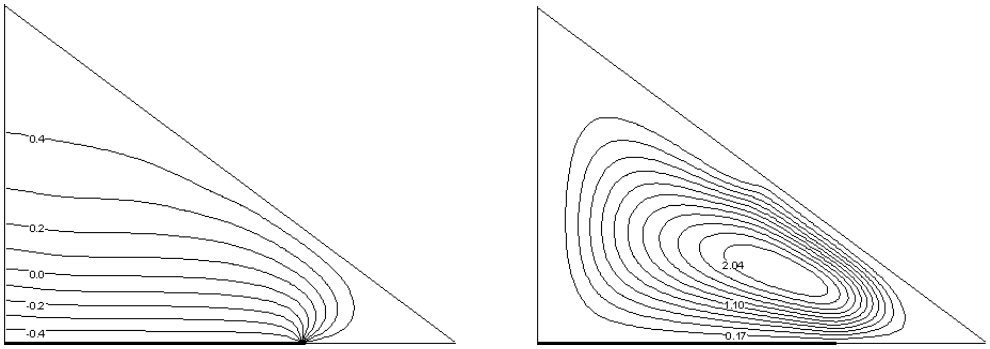

$A = 0.75$

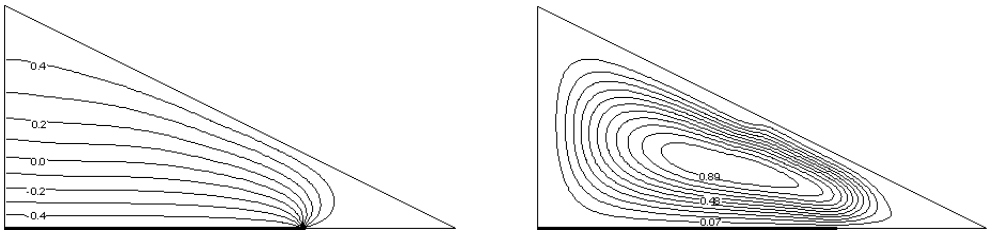

$A = 0.5$

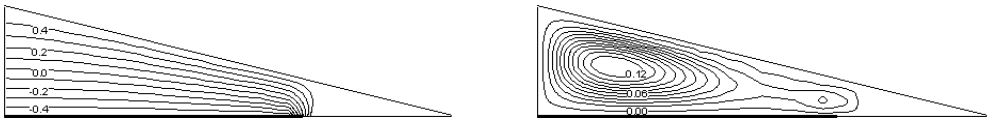

$A = 0.25$

Figure 5.a. Isotherms and streamlines for different aspect ratios for $e^* = 1/3$, $Ra = 10^5$ and $\varepsilon = 0$.

Figure 6 shows the variation of the average Nusselt number *Nuw* according to the Rayleigh number in presence and in absence of the radiation exchange and for different values of aspect ratio.

For the case without radiation (figure 6.a) and for a fixed aspect ratio *A*, it may be observed that when the Rayleigh number increases the average Nusselt number *Nuw* increases. In addition, for a fixed Rayleigh number, when the aspect ratio *A* is increased average Nusselt number decreases. As a matter of fact, the average Nusselt number tend to a unique constant value for aspect ratio $A = 0.25$. We also note that in presence of the radiation exchange (figure 6.b), the average Nusselt number *Nuw* increases according to *Ra* independently of the value of Aspect ratio, this increase is more pronounced comparing to the case of pure nature convection. This can be explained by the fact that the radiation number *Nr* is proportional to Rayleigh number.

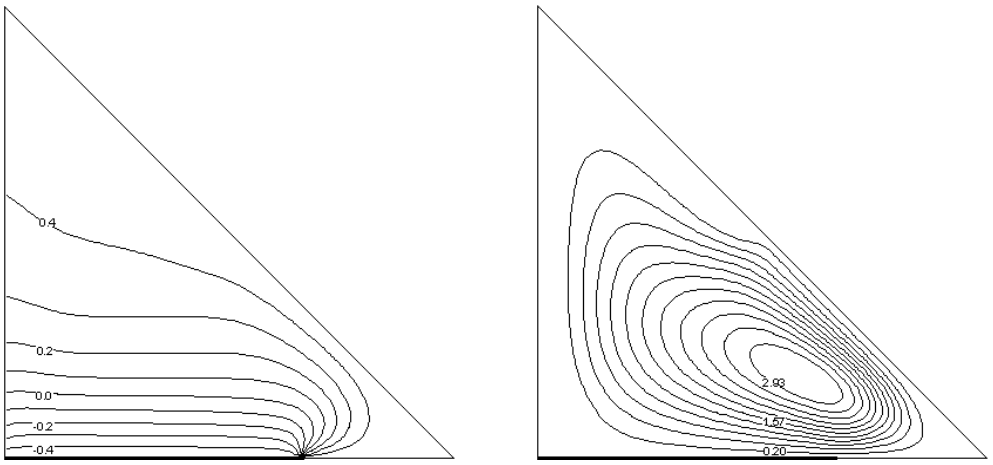

$A = 1$

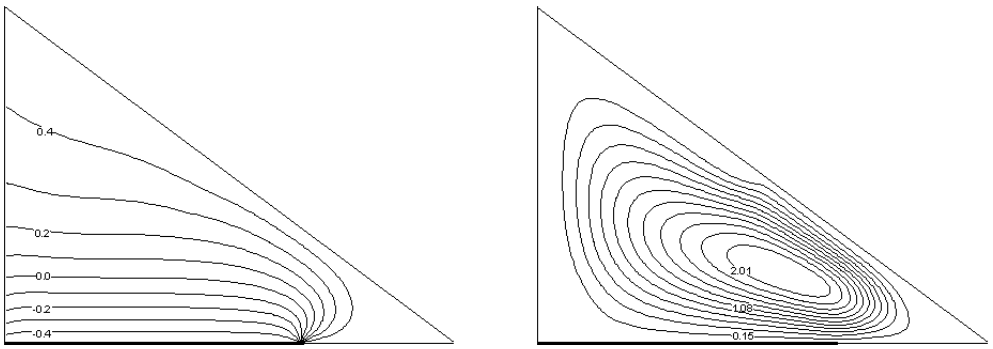

$A = 0.75$

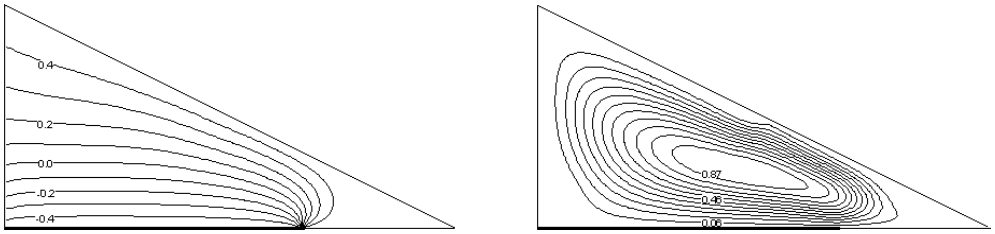

$A = 0.5$

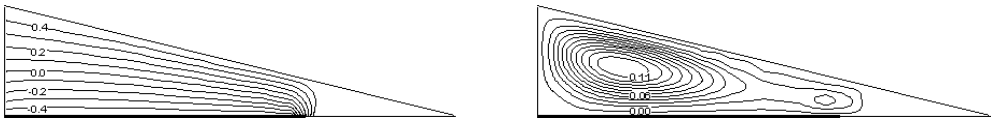

$A = 0.25$

Figure 5.b. Isotherms and streamlines for different aspect ratios for $e^* = 1/3$, $Ra = 10^5$ and $\varepsilon = 1$.

Next the effect of the local Nusselt number *Nu* distribution along the bottom wall is presented in figure 7 in absence and in presence of radiation exchange.

In both cases of pure natural convection (figure 7.a) and combined natural convection to radiation exchange (figure 7.b), the trend of curves is almost the same for all aspect ratio. Also, the curve of $A = 0.25$ is higher than the other curves due to smaller distance between differentially heated walls. Moreover, we can note that for $X \leq 0.66$, the *Nu* remains almost constant. While, the heat transfer improves temporarily from this value presenting the intersection between the bottom wall and the eave and then decreases again to reach zero. Also, it is observed that peak values are high at the smallest aspect ratio. In addition, we reveal from figure 7.b that the local Nusselt number increases comparing to the first case (figure 7.a) due to the presence of radiation exchange

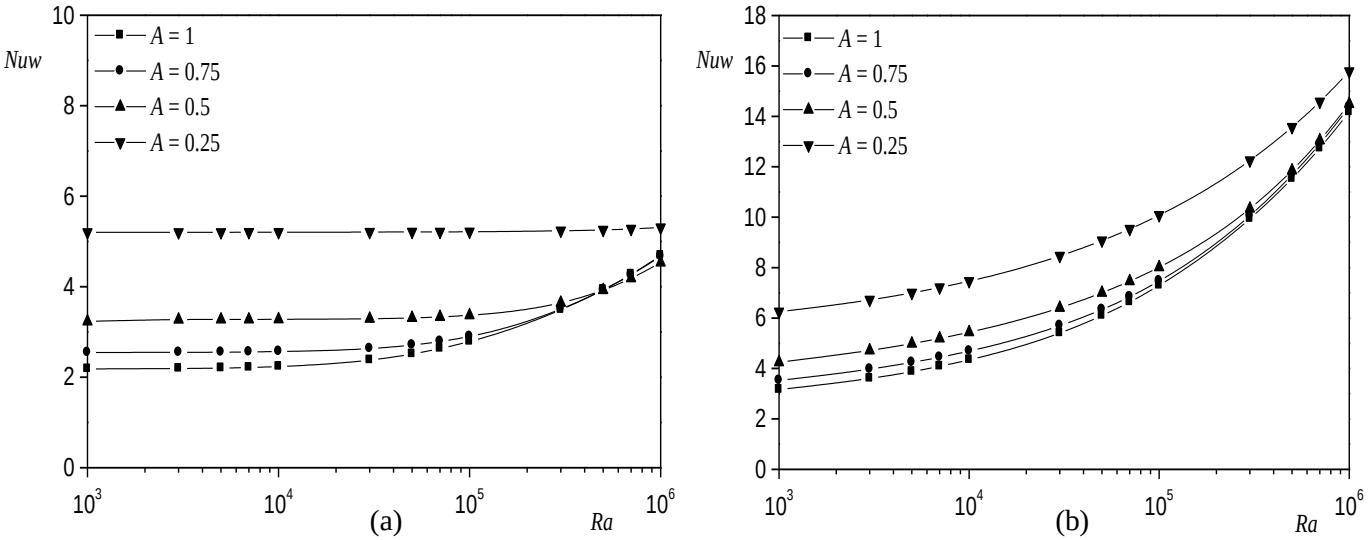

Figure 6. Variation of the average Nusselt number *Nuw* as a function of *Ra* for different *A* and e^* = 1/3: (a) $\varepsilon = 0$, (b) $\varepsilon = 1$.

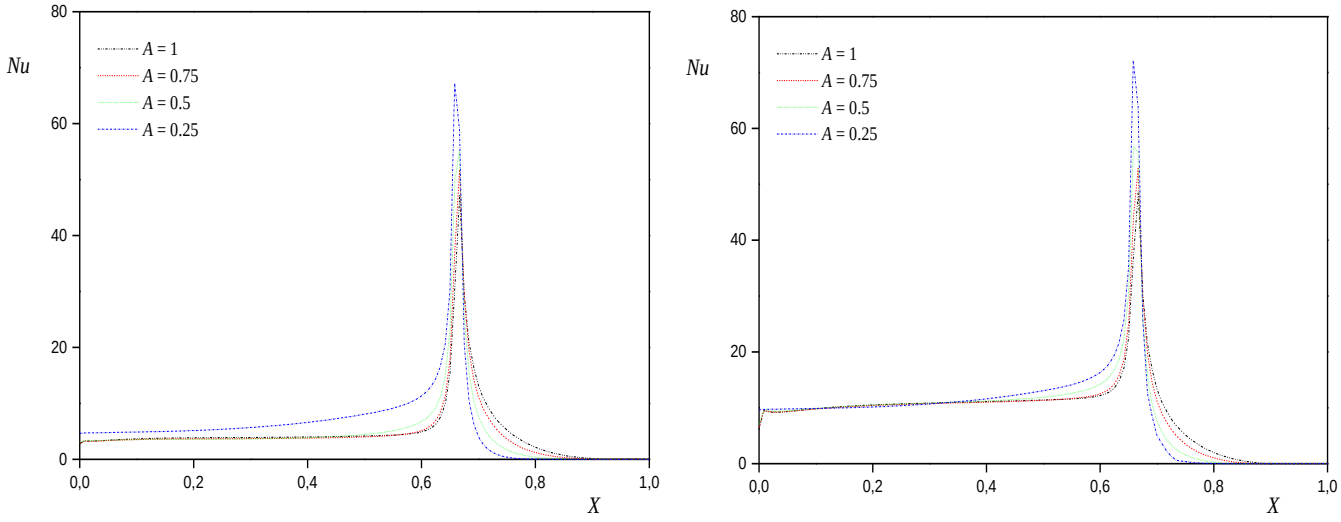

Figure 7. Variation of local Nusselt number for different aspect ratios along the bottom wall for different *A* and e^* = 1/3, $Ra = 10^5$: (a) $\varepsilon = 0$, (b) $\varepsilon = 1$.

3.2.3. *Effect of eave lengths*

In figure 8, we present the flow fields and temperature distribution obtained by the variation of eave length e^* for $A = 0.5$ and $Ra = 10^5$ in absence and in presence of radiation exchange.

As can be seen, in both cases, the eave length has a great effect on flow field and temperature distribution. The streamlines are affected from the intersection of cold bottom wall and starting point of the eave. As the eave length decreases, we can note that the flow goes to right corner of the triangle. In more, the heat transfer per area becomes smaller then the convection strength is increased. The effect of the eave length on heat transfer is presented in Figure 9 for different aspect ratios and for $Ra = 10^6$.

In case without radiation (figure 9.a), it is observed that for a fixed aspect ratio, *Nuw* increases with decreasing eave length e^*. In addition, for a constant e^*, *Nuw* increases with decreasing aspect ratio *A*. However, during the decrease of the eave length, there are significant changes of heat transfer especially for $A = 0.25$.

When the radiation exchange is taken into account (Figure 9.b) the similar trend can be seen. However, the increase of the average Nusselt number is multiplied by two in comparison to the pure natural convection case.

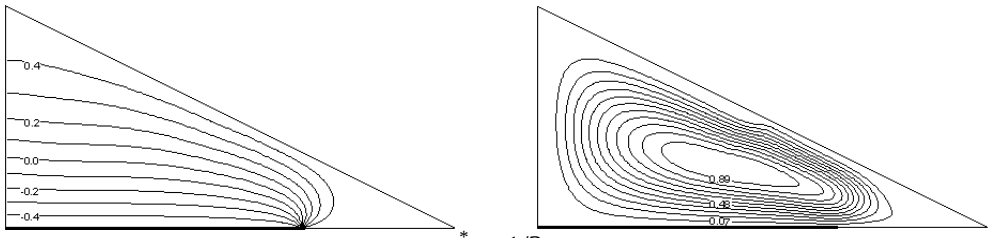

$e^* = 1/3$

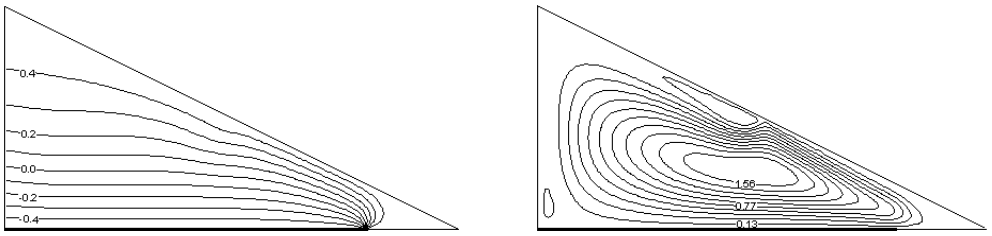

$e^* = 1/5$

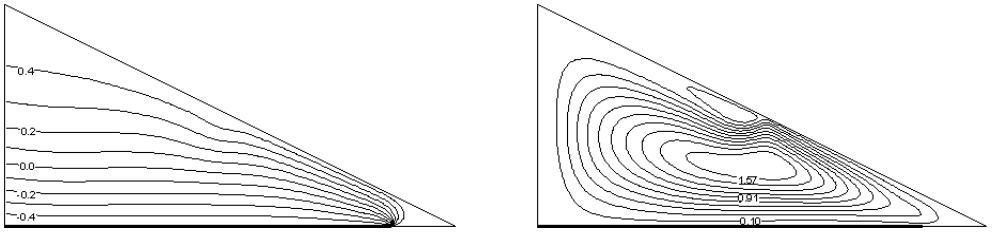

$e^* = 1/7$

Figure 8.a. Isotherms and streamlines for different eave length for $A = 0.5$, $Ra = 10^5$ and $\varepsilon = 0$.

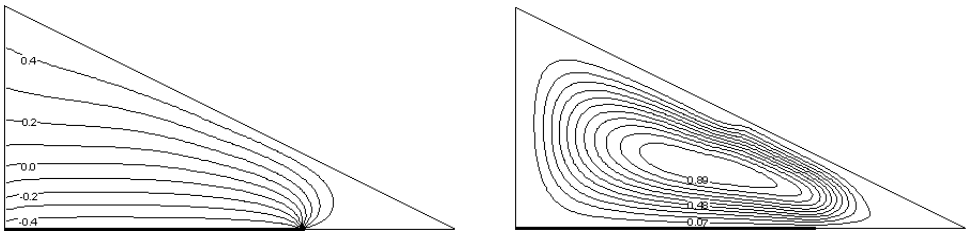

$e^* = 1/3$

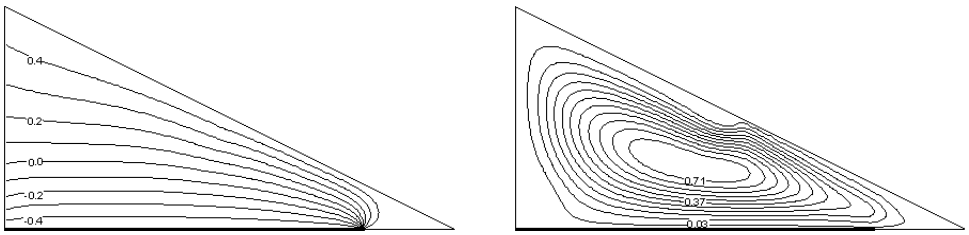

$e^* = 1/5$

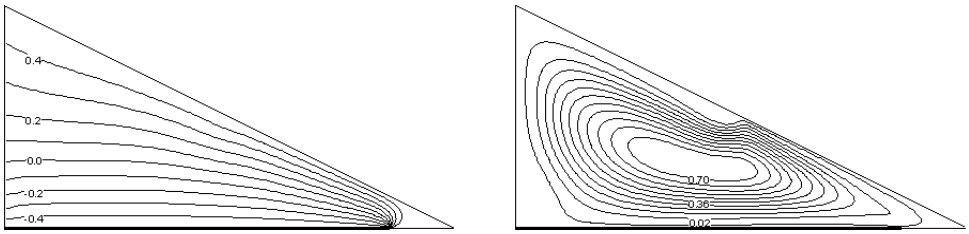

$e^* = 1/7$

Figure 8.b. Isotherms (a) and streamlines for different eave length for $A = 0.5$, $Ra = 10^5$ and $\varepsilon = 1$.

The effect of the eave length on heat transfer is presented in Figure 9 for different aspect ratios and for $Ra = 10^6$. In case without radiation (figure 9.a), it is observed that for a fixed aspect ratio, *Nuw* increases with decreasing eave length e^*. In addition, for a constant e^*, *Nuw* increases with decreasing aspect ratio *A*. However, during the decrease of the eave length, there are significant changes of heat transfer especially for $A = 0.25$.

When the radiation exchange is taken into account (Figure 9.b) the similar trend can be seen. However, the increase of the average Nusselt number is multiplied by two in comparison to the pure natural convection case.

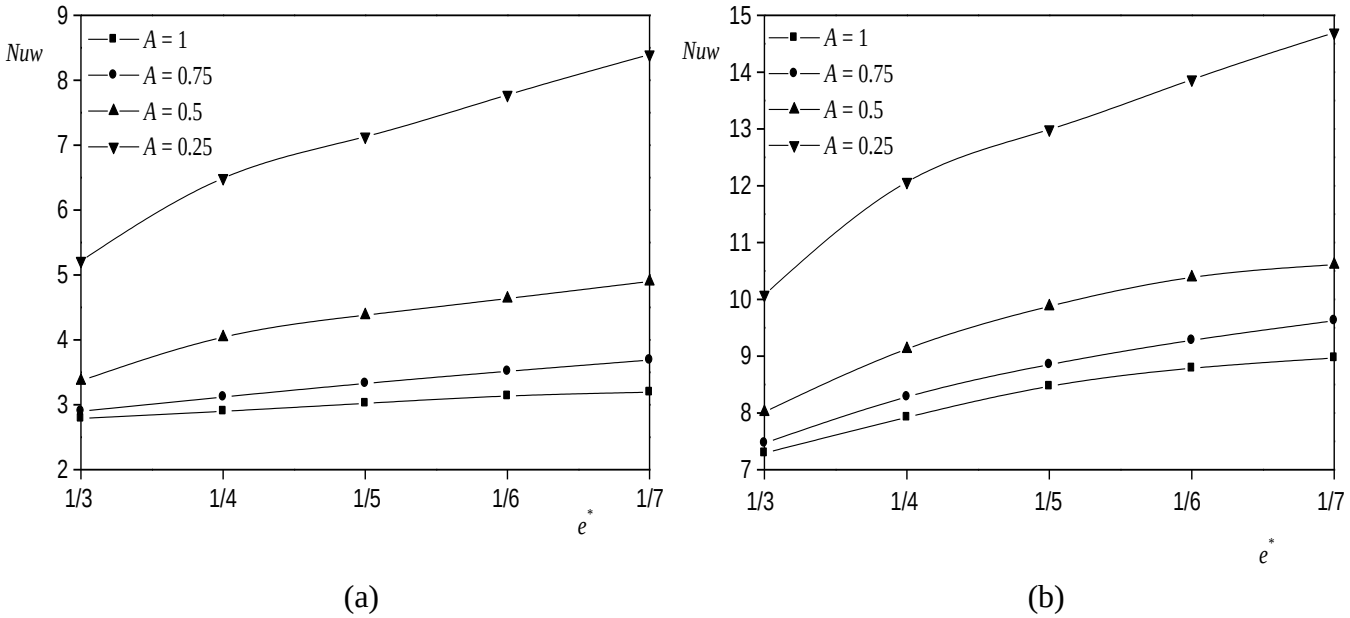

Figure 9. Variation of the average Nusselt number *Nuw* as a function of eave length for different *A* and $Ra = 10^5$: (a) $\varepsilon = 0$, (b) $\varepsilon = 1$.

Figure 10 highlights the impact of increasing the eave length on local Nusselt number along the bottom wall in absence and in presence of radiation exchange. As can be seen, the location of the eave has an important impact on the heat transfer. The local Nusselt number shows wavy variation along the bottom wall and it maximum value depends on the starting eave. Moreover the *Nu* decreases as decreasing eave length, and then the heat transfer is reduced as the opening is moved further to left.

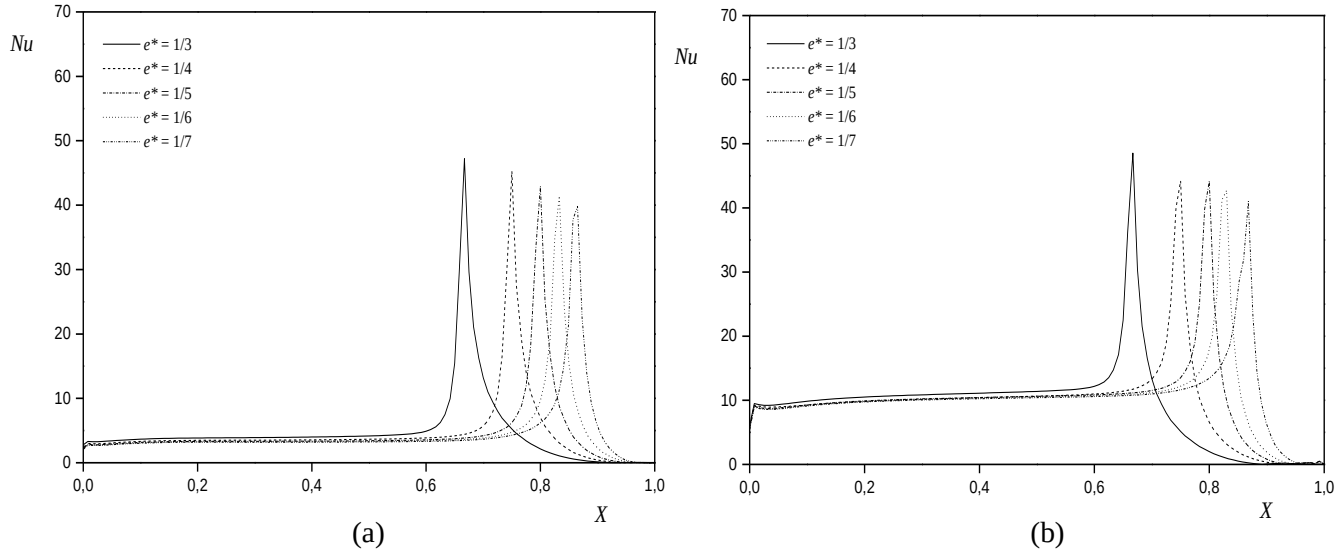

Figure 10. Variation of local Nusselt number for different eave lengths along the bottom wall for $A = 0.5$ and $Ra = 10^5$: (a) $\varepsilon = 0$, (b) $\varepsilon = 1$.

Conclusions

In this work, the treatment of the radiative heat exchanges phenomenon allowed us to get closer to the reality and to better understand the thermal behavior caused by the exchanges between the building walls. In this study we showed the effects of the Rayleigh number, aspect ratio, and eave length on the heat transfer and the air flow in a triangular shaped roof. The principal conclusions obtained lead to:

1. Heat transfer increases with increasing Rayleigh number. However, due to conduction dominant regime, heat transfer is constant for lower Rayleigh numbers.
2. The aspect ratio affects strongly the structure of isotherms and streamlines. For $A = 0.25$, we observe a formation of a secondary rotating cells and the heat transfer is more pronounced where the conduction mode becomes dominant.
3. The heat transfer decreases with increasing eave length.
4. The heat transfer can be controlled by changing the aspect ratio or (and) eave length in order to reduce the heat transfer in roof. So, in order to improve the energy performance in buildings and to reduce the heat exchanges in the enclosure studied, it is necessary to choose the aspect ratio of triangular shaped roof $A \geq 0.5$ for hot climates.

References

1. Haese P. M., Teubner M. D., Heat exchange in an attic space. *Int. J. Heat Mass Transfer*. 45 (25) (2002) 4925-4936.
2. Joudi K. A., Hussein I. A., Farhan A. A., Computational model for a prism shaped storage solar collector with a right triangular cross section. *Energ Convers Manage*. 45 (2004) 337-342.
3. Ridouane E.H., Campo A., Heightened thermal convection as a result of splitting a square cavity diagonally in half. *JEP, Transactions of the ASME*. 128 (3) (2006) 251-258.
4. Lei C., Patterson J. C., A direct-three dimensional numerical simulation of radiation-induced natural convection in a shallow wedge. *Int. J. Heat Mass Transfer*. 46 (2003) 1183-1197.
5. Flack R. D., Konopnicki T. T. and Rooke J. H., The measurement of natural convective heat transfer in triangular enclosures, *J. Heat Trans-T. ASME*. 101 (1979) 648-654.
6. Akinsete V. A. and Coleman T. A., Heat transfer by steady laminar free convection in triangular enclosures. *Int. J. Heat Mass Transfer*. 25 (7) (1982) 991-998.
7. Karyakin Y. U. E., Sokovishin Y. U. A., Transient natural convection in triangular enclosures. *Int. J. Heat Mass Transfer*. 31 (1988) 1759-1766.
8. Kaushik S. C., Kumar R., Garg H. P., Prakash J., Transient analysis of a triangular built in storage solar water heater under winter conditions. *Heat Recovery Systems & CHP*. 14 (4) (1994) 337-341.
9. Salmun H., Convection patterns in a triangular domain, *Int. J. Heat Mass Transfer*. 38 (1995) 351-362.
10. Holtzman G. A., Hill R. W., Ball K. S., Laminar natural convection in isosceles triangular enclosures heated from below and symmetrically cooled from above, *J. Heat Trans-T. ASME*.122 (2000) 485-491.
11. Lei C. W., Patterson J. C., Unsteady natural convection in a triangular enclosure induced by absorption of radiation. *J. Fluid Mech*. 460 (1) (2002) 181-209.
12. Ridouane E. H., Campo A., Relationship between thermal convection intensity and aspect ratio of two triangular cavities inscribed in horizontal rectangular cavities, *Int J. Numer Method H.*16 (2006) 338-355.
13. Varol Y., Koca A., and Oztop H., Natural convection in a triangle enclosure with flush mounted heater on the wall. *Int Commun Heat Mass*. 33 (8) (2006) 951-958.
14. Saha G., Islam T., Saha S., Islam Q., Natural convection in a tilted isosceles triangular enclosure with discrete bottom heating, *Thammasat Int J. Sci Tech.* 12 (2007) 24-35.
15. Koca A., Oztop H. F., Varol Y., The effects of Prandtl number on natural convection in triangular enclosure with localized heating from below. *Int Commun Heat Mass*. 34 (2007) 511-519.
16. Varol Y., Oztop H. F., Yilmaz T., Natural convection in triangular enclosures with protruding isothermal heater. *Int. J. Heat Mass Transfer*. 50 (2007) 2451-2462.
17. Saha S. C., Unsteady natural convection in a triangular enclosure under isothermal heating, *Energ Buildings*.43 (2-3) (2011) 695-703.
18. Asan H. and Namli L., Laminar natural convection in a pitched roof of triangular cross-section: summer day boundary conditions. *Energ Buildings*. 33 (2000) 69-73.

19. Ridouane E. H., Campo A., McGarry M., Numerical computation of buoyant airflows confined to attic spaces under opposing hot and cold wall conditions, *Int J. Therm Sci.* 44 (2005) 944-952.
20. Tzeng S. C., Liou J. H., Jou R. Y., Numerical simulation-aided parametric analysis of natural convection in a roof of triangular enclosures. *Heat Transfer Eng*. 26 (2005) 69-79.
21. Koca A., Numerical investigation of heat transfer with laminar natural convection in different roof types, *PhD Thesis, Firat University, Turkey, Elazig*. (2005).
22. Varol Y., Koca A., Oztop H. F., Laminar natural convection in saltbox roofs for both summerlike and winterlike boundary conditions, *J. Appl Sci*. 6 (12) (2006) 2617-2622.
23. Varol Y., Koca A., Oztop H.F., Natural convection heat transfer in Gambrel roofs, *Build Environ* .42 (2007) 1291-1297.
24. Yadan M., Lei C., Patterson J., Natural convection in a triangular enclosure induced by solar radiation. *16th Australain Fluid Mechanics Conference 2-7 December*. (2007).
25. Sieres J., Campo A., Ridouane E. H., Seara J. F., Effect of surface radiation on buoyant convection in vertical triangular cavities with variable aperture angles. *Int. J. Heat Mass Transfer*. 50 (2007) 5139-5149.
26. Patankar S. V., Numerical heat transfer and fluid flow. *New York, Ny: McGraw-Hill*. (1980).
27. Mezrhab A. and Bouzidi M., Computation of view factors for surfaces of complex shape including screening effects and using a boundary element, *Eng. Computation*. 22 (2) (2005) 132-148.
28. Asan H., Namli L., Numerical simulation of buoyant flow in a roof of triangular cross section under winter day boundary conditions, *Energ Buildings*. 33 (2001) 753-757.
29. Koca A., Hakan , Oztopb F., Varol Y., Numerical analysis of natural convection in shed roofs with eave of buildings for cold climates, *Comput Math Appl*. 56 (2008) 3165-3174.
30. Bouali H., Mezrhab A., Amaoui H., Bouzidi M., Radiation-natural convection heat transfer in an inclined rectangular enclosure, *Int J. Therm Sci.* 45 (2006) 553–566.
31. Mezrhab A., Elfarh L., Naji H., Lemonnier D., Computation of surface radiation and natural convection in a heated horticultural greenhouse, *Appl Energ*. 87 (2010) 894–900.

(2017) ; http://www.jmaterenvironsci.com